Journal of Asian Ceramic Societies 1 (2013) 296–303

Contents lists available at ScienceDirect

Journal of Asian Ceramic Societies

journal homepage: www.elsevier.com/locate/jascer

Controllable hydrogen release via aluminum powder corrosion in calcium hydroxide solutions

Shingo Kanehira[a,*], Susumu Kanamori[b], Kohji Nagashima[b], Takashi Saeki[b], Heidy Visbal[c], Toshimi Fukui[c], Kazuyuki Hirao[b]

[a] Micro/Nano Fabrication Hub, Center for the Promotion of Interdisciplinary, Education and Research, Kyoto University, Yoshida-Honmachi, Sakyo-ku, Kyoto 606-8501, Japan
[b] Department of Material Chemistry, Graduate School of Engineering, Kyoto University, Katsura, Nishikyo-ku, Kyoto 615-8510, Japan
[c] Kansai Research Institute, Inc., 134, Chudoji Minami-machi, Shimogyo-ku, Kyoto 600-8813, Japan

ARTICLE INFO

Article history:
Received 15 March 2013
Received in revised form 3 August 2013
Accepted 4 August 2013
Available online 27 August 2013

Keywords:
Aluminum
Calcium hydroxide
Hydration
Katoite
Hydrogen

ABSTRACT

Mechanism of aluminum powder corrosion in calcium hydroxide solutions was investigated via various analyses of residues after its hydrolysis reaction and pH change of the solutions to control the release of hydrogen gas. It was revealed that the reaction with a release of hydrogen gas consisted of katoite formation and hydration of aluminum. The katoite formation, which is progressed by the reaction among calcium ion, aluminum hydroxide anion ($Al(OH)_4^-$), and water molecules at the first step, is important for the promotion of aluminum corrosion and moderate release of hydrogen gas.

1. Introduction

Hydrogen is one of the important energy resources that can be consumed in a fuel cell, converting chemical energy into electrical energy with a high performance. Fuel cells, operating with hydrogen or hydrogen-rich fuels, have the potential to become major factors in catalyzing the transition to a future sustainable energy system with low CO_2 emissions [1]. In general, hydrogen gas is mainly produced in large quantities by steam reforming of hydrocarbons, such as methane. The produced gas should be compressed at 200 bar in a high-pressure tank for the storage. Another storage method for the hydrogen gas is to use the chemical reaction between water and metal hydrides, including lithium hydride (LiH), sodium hydride (NaH), lithium tetrahydridoborate ($LiBH_4$), and sodium tetrahydridoborate ($NaBH_4$) [2]. Almost all hydrides shown above are stable in dry or ambient air, however, when water eventually diffuses into the hydride, the hydration reaction accelerates and it will be out of control because these reactions are highly exothermic and potentially dangerous. Therefore, the reaction at which water is combined with the chemical hydride should be precisely controlled to avoid these runaway reactions and potential explosion.

Another possible method for the hydrogen gas generation is the procedure based on a corrosion of base metal such as aluminum in solutions. Hydrogen production from aluminum can provide an alternative means to produce pure hydrogen for feeding to a micro-fuel cell. The basic possible aluminum oxidation reactions in water are the following:

$$Al + 3H_2O \rightarrow Al(OH)_3 + 3/2H_2 \quad (1)$$

$$Al + 2H_2O \rightarrow AlOOH + 3/2H_2 \quad (2)$$

$$Al + 3/2H_2O \rightarrow 1/2Al_2O_3 + 3/2H_2 \quad (3)$$

All the reactions are accompanied by the release of hydrogen and solid byproducts such as bayerite [$Al(OH)_3$], boehmite [AlO(OH)], and aluminum oxide [Al_2O_3]. The advantages of using aluminum powder for the hydrogen generation exist in cost effective, high efficiency, pure hydrogen generation with high humidity, and simple changeability [3]. The reactions shown above are thermodynamically favorable; however, the presence of a passive layer

* Corresponding author. Present address: Ecotopia Science Institute, Nagoya University, Furo-Cho, Chikusa, Nagoya 464-8603, Japan. Tel.: +81 52 789 3913; fax: +81 52 789 3910.
E-mail address: kane@esi.nagoya-u.ac.jp (S. Kanehira).

Peer review under responsibility of The Ceramic Society of Japan and the Korean Ceramic Society.

Production and hosting by Elsevier

2187-0764 © 2013 The Ceramic Society of Japan and the Korean Ceramic Society. Production and hosting by Elsevier B.V. All rights reserved.
http://dx.doi.org/10.1016/j.jascer.2013.08.001

containing oxides at the surface prevents the reaction between water and aluminum. Therefore, the hydration reaction of pure aluminum cannot proceed completely in water without any additives. Many reports claimed that sodium hydroxide acts as a catalyst to proceed the hydrogenating reaction in the following reaction:

$$Al + 3H_2O + NaOH \rightarrow NaAl(OH)_4 + 3/2H_2 \quad (4)$$

$$NaAl(OH)_4 \rightarrow NaOH + Al(OH)_3 \quad (5)$$

The main disadvantage using NaOH solutions was that the employment of strong corrosive agent is harmful to handle and difficulty of reaction control: the strong base tends to initiate the runaway reaction. Soler et al. [4,5] reported the hydrogen production curve from the hydrolysis reaction of pure aluminum or various aluminum alloys with different additives. They concluded that the base, its concentration, and temperature affected the hydrogen production rate. In order to apply the aluminum corrosion process into the source of hydrogen for fuel cell applications, it needs to clarify the mechanism of corrosion. In addition, the controllable hydrogen gas release, especially, the moderate evolution of the gas is also important for the wide application of fuel cells.

Here, we demonstrated the control of hydrogen gas release in calcium hydroxide ($Ca(OH)_2$) solutions and analyzed the corrosion mechanism of pure aluminum powder. Calcium hydroxide was selected as a base to ignite the corrosion reactions with a safer pH even at saturation level (pH = 12.6) and easy to control not only the amount of hydrogen but also the speed of hydrogen release. The detailed investigation of residues using various surface analysis methods revealed the corrosion mechanism in the $Ca(OH)_2$ solutions.

2. Experimental procedure

Raw materials used in the present work were mixture of aluminum powder (>99.99%, φ = ~40 μm, Kojundo Chemical) and calcium hydroxide, $Ca(OH)_2$ (>95.0%, Nacalai Tesque). The $Ca(OH)_2$ powder is added to remove the surface oxide and ignite hydration reaction of aluminum powder. The weight ratio (wt.%) of the sample mixture, Al/$Ca(OH)_2$, was set to 80/20(Al80_Ca20), 70/30(Al70_Ca30), and 50/50(Al50_Ca50), respectively. The reactants were prepared via mixing in the mortar, and each reactant of 18 g in weight was set in the glass pot of 500 mL. Fig. 1 indicates a schematic illustration of the measurement system of the hydrogen gas generation. A distilled water of 200 mL in volume was poured into the pot and hydration reaction was initiated inside. The sample mixture was stirred using a magnetic stirrer to prevent the solidification of the product and promote the hydration reaction. Each concentration of $Ca(OH)_2$ solution of Al80_Ca20, Al70_Ca30, and Al50_Ca50 is calculated to be 0.25, 0.37, and 0.60 mol/L, respectively. The temperature change of the solutions was monitored using K-type thermocouple. The released gas during the reaction flew through a glass tube with ~8 mm diameter and bubbled into the water through a glass wool. The evolution rate of hydrogen gas was monitored using a flow meter and was converted into the total volume (mL) of the gas. The component of the discharged gas was analyzed using gas chromatograph (GC-2014, Shimadzu Corporation, Japan). We used high-purity argon gas (99.99%) and SHINCARBON ST 50-80 as a carrier gas and a column in the analysis.

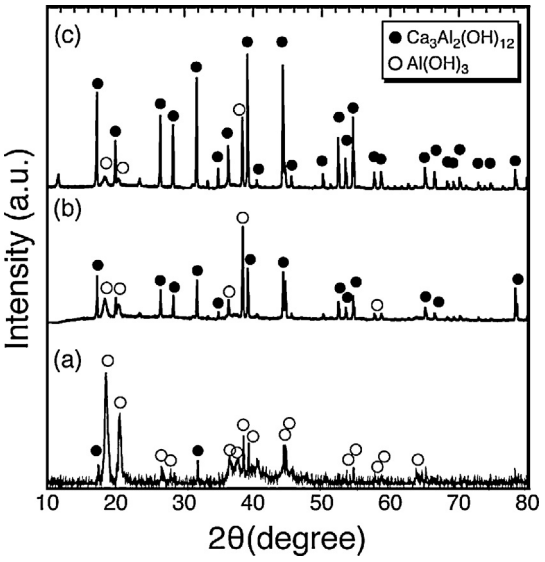

Fig. 2. XRD patterns of residues after the hydration reactions of the sample (a) Al80_Ca20, (b) Al70_Ca30, and (c) Al50_Ca50, respectively.

Residual mixture was filtered through a fine filter paper and dried for 24 h at 80 °C inside an oven. The dried mixture was ground to a fine powder using a mortar. X-ray diffraction (XRD) patterns of the sample powder were recorded on X-ray diffractometer (RINT2500, Rigaku, Japan) with CuKα radiation for identification of their crystal structure. The microstructure of the mixture was

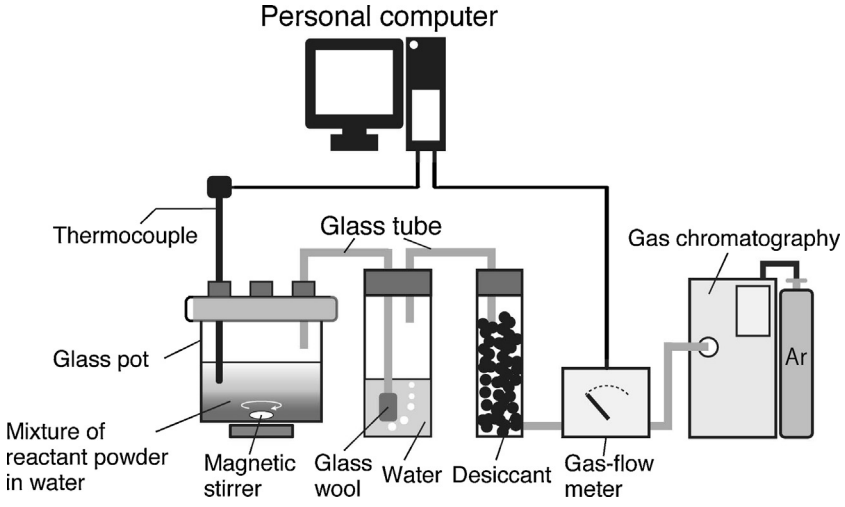

Fig. 1. Schematic illustrations of measurement system of hydrogen gas release via aluminum corrosion.

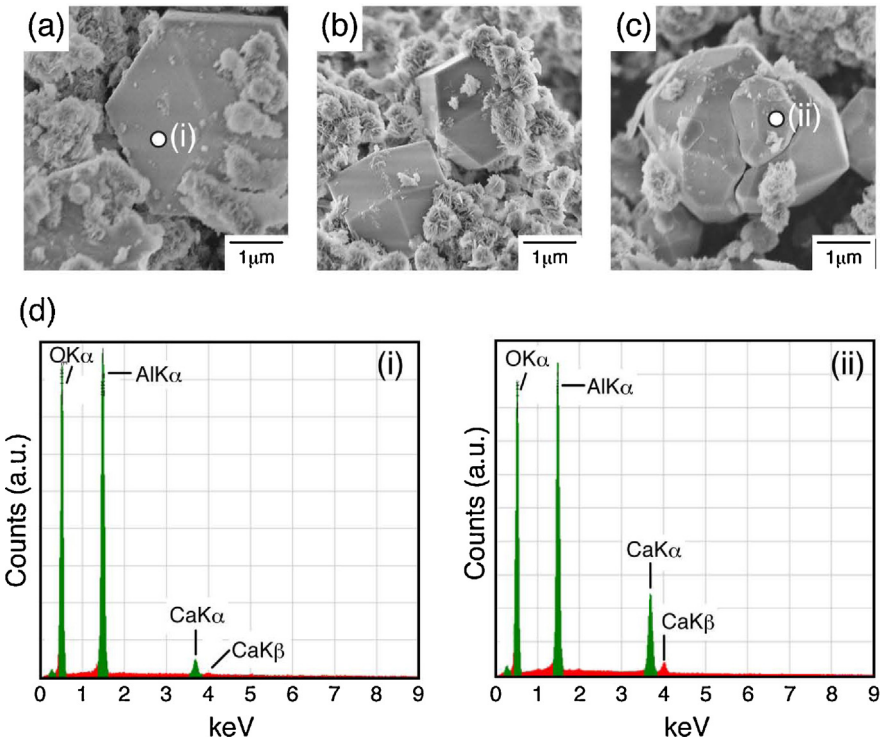

Fig. 3. FE-SEM photos of the hydrated samples of (a) Al80_Ca20, (b) Al70_Ca30, and (c) Al50_Ca50, respectively. EDX signals at the point of (i) and (ii) in (a) and (c) are shown in (d-i) and (d-ii), respectively.

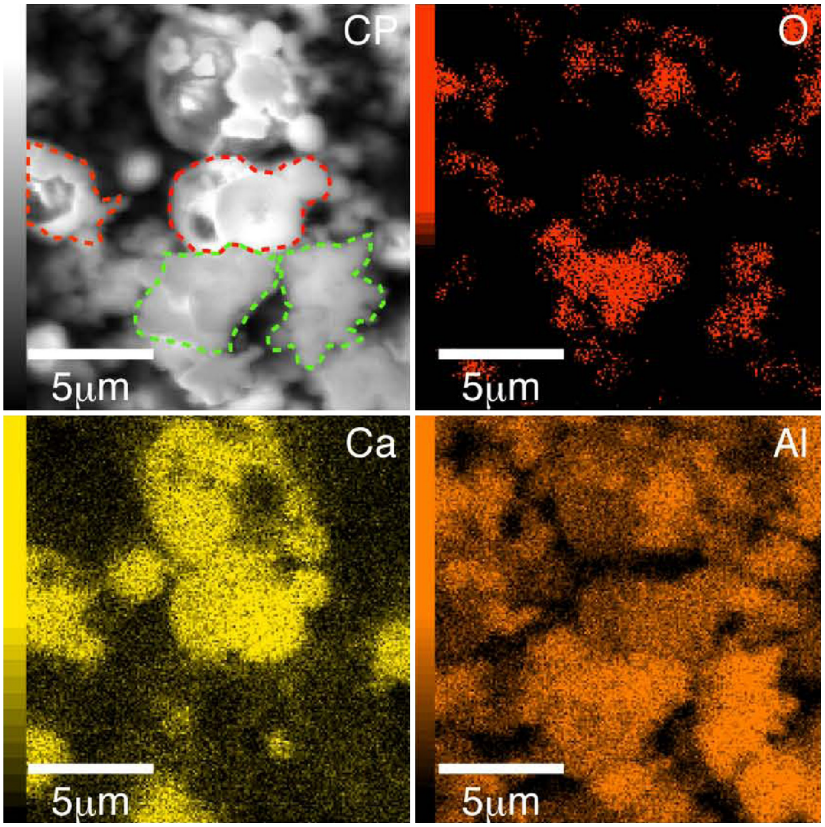

Fig. 4. Elementary distribution of oxygen, calcium, and aluminum in the hydrated samples of Al50_Ca50. CP indicates compo image. The areas surrounded by red or green broken lines show katoite or $Al(OH)_3$ particles, respectively.

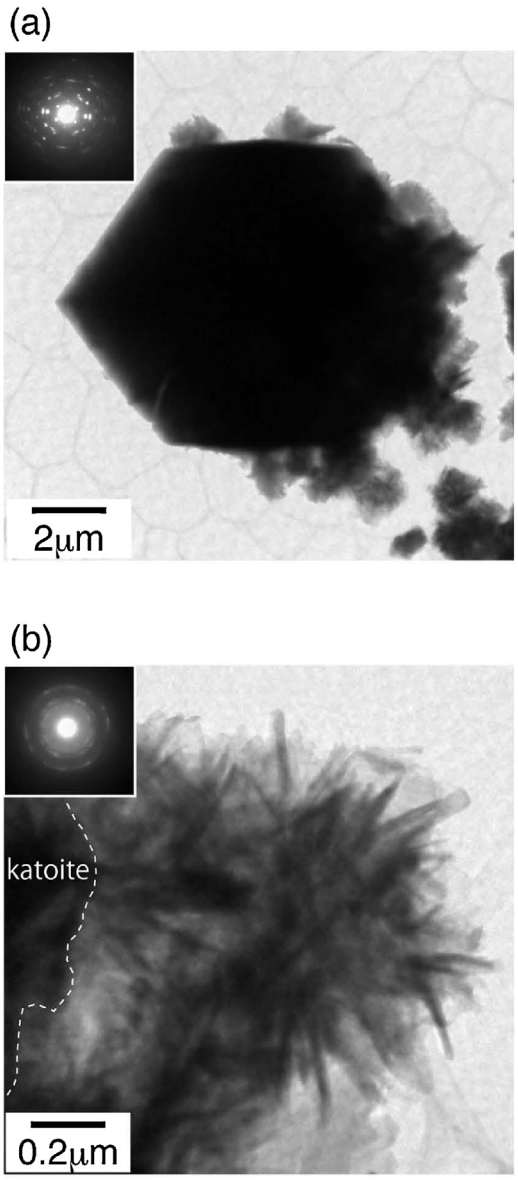

Fig. 5. TEM image of (a) katoite and (b) $Al(OH)_3$ area containing the dried residue of Al80_Ca20 that were obtained after the hydration reaction, respectively. The corresponding selected-area electron diffraction (SAED) patterns taken from each body are also inserted in the left corner.

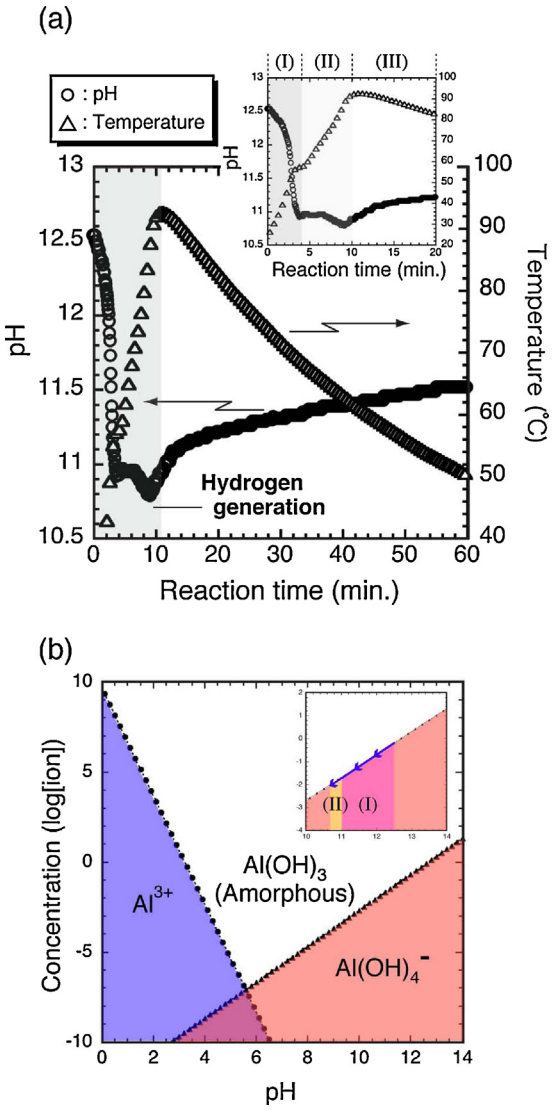

Fig. 6. (a) The plots of pH and temperature of the solution containing Al50_Ca50 sample. Magnification between the start and 20 min is shown at the corner of the same figure. (b) Calculated aluminum solubility diagram in equilibrium with amorphous $Al(OH)_3$ in 25 °C. The inset at the corner indicates an enlarged diagram between pH = 10 and 14.

observed using field-emission type secondary electron microscope (FE-SEM, JEOL, JSM6705F). The atomic distribution at the crystal was identified using energy dispersive X-ray spectroscopy (EDX) that was attached with the FE-SEM apparatus to distinguish the product mixture. High-resolution photo of the residual particles was observed using a transmission electron microscope (TEM, JEOL, JEM-2100F, 200 kV). The powder was dispersed in the ethanol, skimmed from the solution using copper grid. The change of pH during the hydration reaction was monitored using pH meter.

3. Results and discussions

Fig. 2 shows XRD patterns obtained from the products after the hydration reaction of reactant mixtures; (a) Al80_Ca20, (b) Al70_Ca30, and (c) Al50_Ca50. In Fig. 2(a), the product was mainly composed of bayerite [$Al(OH)_3$]. The broad peaks originated from bayerite, especially at $2\theta = 37–40^\circ$, were due to the mixture of amorphous and crystalline phases. Some peaks originating from katoite, $Ca_3Al_2[(OH)_4]_3$, were also detected in the spectrum. The katoite has a cubic structure with *Ia3d* space group, the same as grossular $Ca_3Al_2[SiO_4]_3$. The hydrogrossular series, $Ca_3Al_2[SiO_4]_3$ and $Ca_3Al_2[(OH)_4]_3$, can accommodate large quantities of water [6,7]. The products including katoite might contain the water inside the lattice during the hydration reaction. The peak intensity of katoite became stronger in Fig. 2(b) than that shown in Fig. 2(a), and the main product in Fig. 2(c) was katoite which had high crystallinity. Volume ratio of katoite in the products gradually increases as the ratio of $Ca(OH)_2$ in the reactant increases from Fig. 2(a) to (c). We have confirmed that almost all the reactants were converted into katoite after the hydration reaction when the weight ratio of $Ca(OH)_2$ increased up to 70 wt.%. The products after the hydration reaction were insoluble and cement-like adhesive powder with a gray color, and tended to adhere at the bottom of glass pot.

SEM photos of the residues after the hydration reaction of Al80_Ca20, Al70_Ca30, and Al50_Ca50 samples are shown in Fig. 3(a)–(c), respectively. The crystal which had hexagonal shape

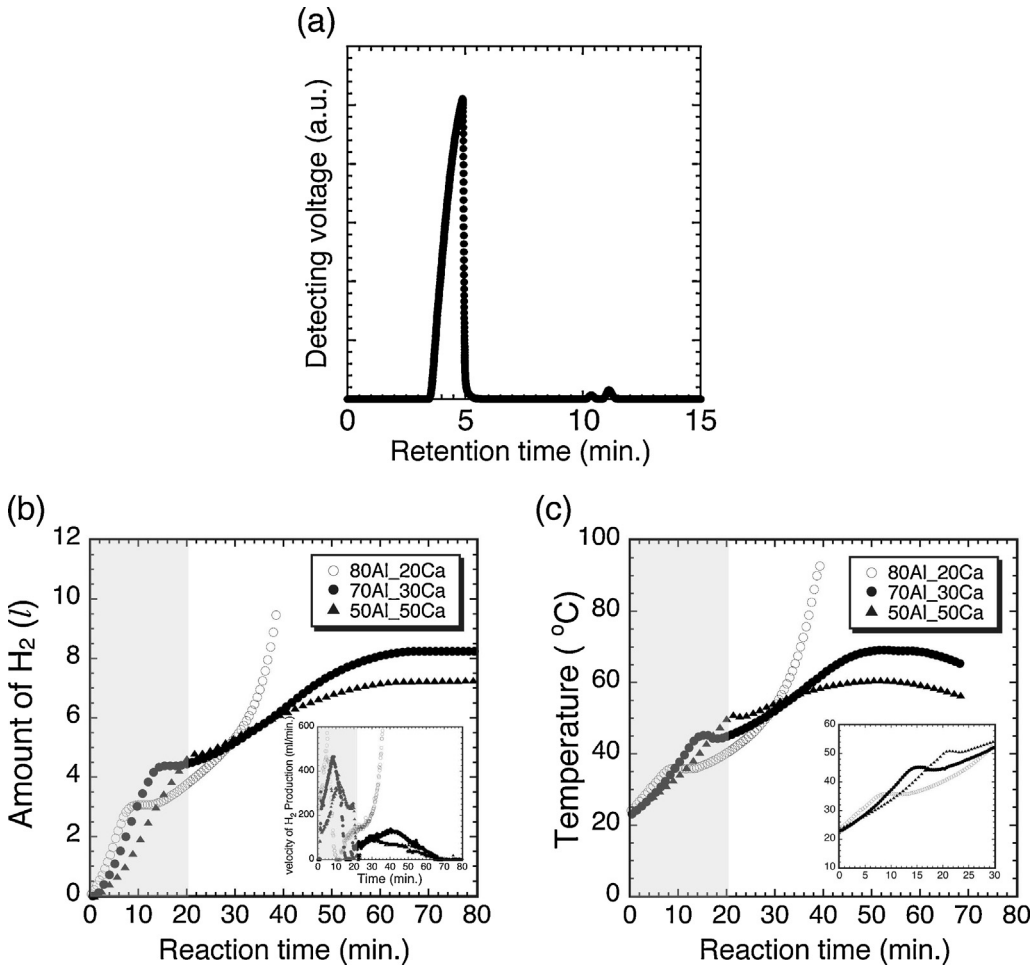

Fig. 7. (a) A plotted curve obtained from a gas chromatography during the hydration reaction. (b) Volume change of hydrogen gas about Al80_Ca20, Al70_Ca30, and Al50_Ca50 obtained from gas flow meter. Each change of the solution temperature containing the samples is also shown in (c).

crystal with a diameter of 2–3 μm might indicate the katoite because the katoite is classified as cubic class with high symmetry. The katoite crystals were surrounded with another small sediment that had whisker shape with a dimension under ~800 nm. XRD spectra in Fig. 2 indicated that the whisker might be identified as $Al(OH)_3$ phase. EDX spectra obtained from the point focused on the katoite crystals in Fig. 3(a) and (c) are shown in Fig. 3(d-i) and (d-ii), respectively. Four peaks attributed to OKα, AlKα, CaKα and CaKβ were detected at 0.5, 1.5, 3.6 and 4.0 keV, respectively. However, both the CaKα and CaKβ peaks were not detected at the whisker. The peak of CaKα and CaKβ in Fig. 3(d-ii) is larger than that in Fig. 3(d-i) depending on the weight ratio of $Ca(OH)_2$; therefore, the hexagonal crystal could be identified to be katoite. In addition, the shape of the katoite crystal changed from hexagonal into polyhedron. The shape or size of whisker originated from $Al(OH)_3$ was almost the same among each sample.

Fig. 4 shows a distribution of aluminum, calcium, and oxygen ions of hydrated residues composing katoite and $Al(OH)_3$ at the area of 15 μm × 15 μm. Each area surrounded by red or green broken lines in CP image is crystalline hexagonal phase and whisker, respectively. The red area showed the distribution of Al, Ca, and O ions; however, the green one showed the existence of Al and O ions only. It was estimated that the hexagonal (red) and whisker (green) area showed katoite and $Al(OH)_3$, respectively, because the Ca ion exists only at the katoite particle.

Fig. 5 shows TEM photos of (a) katoite and (b) $Al(OH)_3$ containing the dried residue of Al80_Ca20 after the hydration reaction. The corresponding selected-area electron diffraction (SAED) patterns are also inserted at the left corner of each photo. The katoite had a hexagonal with a diameter of 10 μm and showed polycrystalline. The katoite was surrounded with $Al(OH)_3$ powder precipitated in the solution. The SAED pattern taken from the surrounding $Al(OH)_3$ whisker in Fig. 5(b) showed broad and blurred diffraction rings, presumably due to a mixture of amorphous and polycrystalline phases. These results were consistent with existence of amorphous and crystalline phases in the XRD patterns in Fig. 2(a).

Fig. 6(a) indicates the change of pH (circle) and the temperature of solution (triangle) during the hydration reaction. The magnification until 20 min was also shown at the upper corner. The $Ca(OH)_2$ has poor solubility in the water (0.17 g/100 mL at 25 °C) in comparison with NaOH and its saturated solution shows at most pH 12.4–12.5 at room temperature. The hydrogen gas generated vigorously until 10 min and it gradually decreased below the lower limit of the flow meter. The pH plots could be divided into three terms: I (0–4 min), II (4–10 min), and III (10 min ~ end). At first, the pH showed 12.5 and it suddenly dropped into 10.9 within 4 min due to the consumption of —OH ions. On the term II, the pH kept the same value and slightly decreased into 10.7. On the term III, it gradually increased as the solution temperature decreased and reached 11.5. The amorphous $Al(OH)_3$ shown in Fig. 5(b) is known for its amphoteric characteristic, resolving in either strong acid or alkali solution as follows:

$$Al(OH)_3 + 3H^+ \rightleftarrows Al^{3+} + 3H_2O \quad (6)$$

$$Al(OH)_3 + OH \rightleftarrows Al(OH)_4 \quad (7)$$

Fig. 6(b) shows the calculated the aluminum solubility diagram in equilibrium with amorphous $Al(OH)_3$ at 25 °C based on the equilibrium (6) and (7). The inset at the corner indicates the enlarged ion concentration between pH = 10 and 14 in the same diagram. The aluminum solubility during the terms I and II in Fig. 6(a) corresponds to the magnification in the inset in Fig. 6(b). It was clear that the aluminum solubility depended on the pH change strongly. The water molecules in the hydration shell are progressively replaced by hydroxyl ions, giving negative charge, according to the following sequence:

$$Al^{3+} \rightarrow Al(OH)^{2+} \rightarrow Al(OH)_2{}^{+} \rightarrow Al(OH)_3 \rightarrow Al(OH)_4{}^{-} \quad (8)$$

The hydrolysis scheme above would proceed from left to right as the pH increased [8]. The soluble anion $Al(OH)_4{}^-$ becomes dominant in our experiment considering the change of pH from 12.5 to 10.7 in Fig. 6(a). The insoluble $Al(OH)_3$ would precipitate as the pH of the solution decreased. The temperature of the mixture increased up to ~94 °C within 10 min with a plateau at 3 min with an evolution of hydrogen gas, and it gradually decreased after the generation of hydrogen gas ended. Then, we could estimate that more than two chemical reactions progressed with a generation of hydrogen gas.

Fig. 7(a) indicates a general appearance of plotted curves obtained from a gas chromatography during the hydration reaction. The strong peak at 4.90 min, small dips at 10.3 and 11.1 min in the retention time show hydrogen, nitrogen and oxygen gas, respectively. That is, almost all the produced gas during the reaction was identified as hydrogen. The N_2 and O_2 peaks are due to the mixture of residual air from the glass pot. Fig. 7(b) shows a volume change of hydrogen gas about Al80_Ca20, Al70_Ca30, and Al50_Ca50 as a function of reaction time. The change of the velocity of hydrogen gas generation (mL/min) is also plotted at the right corner of the figure. In case of 80Al_20Ca, we stopped the reaction at 40 min due to the dangerous runaway reaction derived from the corrosion of excess aluminum powder. The profile of the volume change can be divided into two terms: 0–20 min (shade area) and 20–80 min. (The hydrogen gas generation was completed at 70 min.) The maximum of the velocity of hydrogen gas generation within 8–11 min decreased from 460 to 360 mL/min as shown in the inserted figure when the weight ratio of aluminum in the reactant powder decreased from 70Al_30Ca to 50Al_50Ca. However, both reaction rates in 70Al_30Ca and 50Al_50Ca showed more than 99% calculated from the total volume of the hydrogen gas. The reaction rate of 80Al_20Ca was calculated to be 95% at most.

Fig. 7(c) shows the temperature dependence of the solutions as a function of reaction time. The magnification till ~30 min is also shown at the corner. In case of 80Al_20Ca, the temperature increased from 23 °C to 45 °C within 10 min, shown within the shaded area, and runaway reaction started. In case of other samples, the temperature increased for more than 15 min and showed a plateau term. Moreover, it increased again and reached at 60 °C (50Al_50Ca) or 70 °C (70Al_30Ca) after 50–60 min.

Each XRD profile of the sample Al50_Ca50 at 7, 35, and 65 min later in Fig. 8(I) was shown in Fig. 8II(a), (b), and (c), respectively. These samples were prepared by filtering the sample using a filter paper to remove the water at each time. Both $Al(OH)_3$ and katoite were produced within the term (a), however, the main component was identified as unreacted aluminum. At the term (b), the ratio of katoite increased and the unreacted aluminum decreased. At the term (c), almost all products were identified as katoite and $Al(OH)_3$ and unreacted aluminum was not observed. In addition, the amount of $Al(OH)_3$ was increased from Fig. 8II(b) to (c).

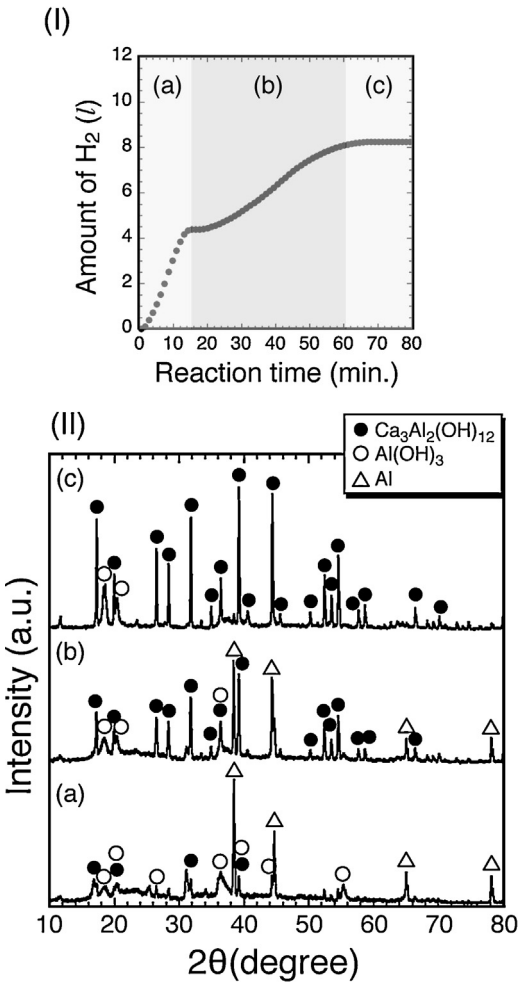

Fig. 8. (I) Typical volume change of hydrogen gas as a function of time. XRD patterns of the residues left after the hydration reaction at (a) 7, (b) 35, and (c) 65 min later within I(a)–(c) are shown in II(a)–(c), respectively.

Fig. 9 shows a model of the chemical reactions in the mixture. We suppose that the corrosion reactions would proceed from the stage 1 to 4. Considering the existence of surface oxide on the surface of aluminum particle, we propose the following equilibrium reactions at the stage 1 and 2:

$$Al_2O_3 + H_2O \rightleftarrows 2AlOOH \quad (9)$$

$$AlOOH + H_2O \rightleftarrows Al(OH)_3 \quad (10)$$

$$Al(OH)_3 + OH \rightleftarrows Al(OH)_4{}^- \quad (11)$$

$$3Ca^{2+} + 2Al(OH)_4 + 8H_2O \rightleftarrows Ca_3Al_2(OH)_{12} + 6H_2 \quad (12)$$

Suppose that the Al_2O_3 shown in (9) is different from bulk α-Al_2O_3 with a corundum structure [9]. The thin passive layer reacted with water and disruption of Al—O—Al bonds occurs via hydrolysis reaction to form Al-OH species. The alkali solution accelerated the reaction effectively. It was reported that one Al–O–Al linkage is broken to form two Al-OH for each water molecule consumed in the hydrolysis reaction [9]. The water molecule tends to attack the aluminum through the pits that contain the passive layer and hydration reaction proceeded. Then, extensive hydration propagates the formation of boehmite, γ-AlOOH, or aluminum hydroxide, $Al(OH)_3$, that are thermodynamically more stable than Al_2O_3 at room temperature in hot water following (9) and (10) [10]. The amorphous $Al(OH)_3$ tends to dissolve into $Al(OH)_4{}^-$ ion

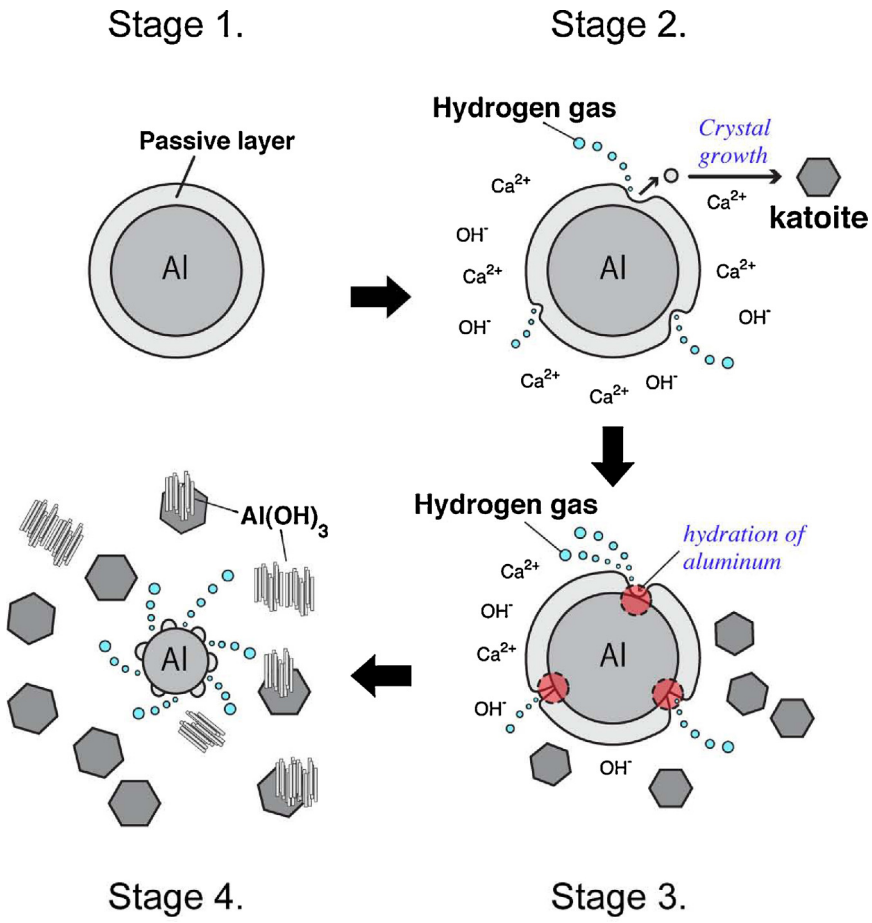

Fig. 9. Model of the aluminum corrosion in $Ca(OH)_2$ solution. The corrosion reactions progress from the stage 1 to 4.

in strong alkali solutions as shown in (11), resulting in the formation of seeds and the growth of katoite via the reaction among Ca^{2+}, $Al(OH)_4^-$ ions and water molecule following the reaction (12). One of the characteristics of the chemical reaction is in the easy controllability of the speed of hydrogen release by controlling the reactions shown in (9)–(12). In Fig. 7(b), the term between the start and the first shoulder in the curve, as shown in the shaded area, increased in proportion to the increase of weight ratio of $Ca(OH)_2$ in the starting material due to the progress of katoite formation shown in the stage 1 and 2 in Fig. 9.

At the stage 3, hydration of aluminum powder mainly progressed with the release of hydrogen gas following the reactions (1)–(3) after the surface oxide dissolved into the solution and localized breakdown occurred shown in the figure (red circle). The aluminum hydration further progressed and the bare aluminum was converted into insoluble $Al(OH)_3$, which had a whisker shape, and polycrystalline katoite crystals in Fig. 3(a)–(c). As these reactions proceeded, the size of aluminum decreased as shown in the stage 4 and it finally dissolved into the solutions completely and the release of hydrogen stopped.

The weight ratio of the $Ca(OH)_2$ is one of the important factors to release the hydrogen gas from the corrosion reaction of aluminum powder. The initial pH in the solution was almost the same in all the samples; however, the reaction rate of the aluminum corrosion depended on $Ca(OH)_2$ content. The release of hydrogen gas was originated from both the katoite formation and hydration of aluminum. The OH— ion helps the destruction of passive layer at the surface of aluminum powder and makes a pit to pass the water molecule. However, the aluminum hydration produces gel-like amorphous $Al(OH)_3$ to obstruct the pit, resulting in the termination of the reaction. In addition, the lack of $Ca(OH)_2$ tended to promote the runaway reaction as shown in 80Al_20Ca sample. That is, the appropriate addition of $Ca(OH)_2$ promotes the crystal growth of katoite shown in stage 2 in Fig. 9, and realized the good controllability of aluminum corrosion with the moderate release of hydrogen gas.

4. Conclusions

We demonstrated the controllable hydrogen release via the corrosion of aluminum powder in $Ca(OH)_2$ solutions. The corrosion mechanism of the aluminum in the solution was analyzed using various surface analyses of residues and the plot of pH change in the solution in detail. It was estimated that the mechanism included katoite formation and hydration of aluminum; the katoite formation has an important factor to proceed with the aluminum corrosion and generate the hydrogen gas moderately.

Acknowledgements

This work was supported by Regional Innovation Strategy Support Program from the Ministry of Education, Culture, Sports, Science and Technology.

References

[1] P.P. Edwards, V.L. Kuznetsov, W.I.F. David and N.P. Brandon, Energy Policy, 36, 4356–4362 (2008).

[2] V.C.Y. Kong, F.R. Foulkes, D.W. Kirk and J.T. Hinatsu, Int. J. Hydrogen Energy, 24, 665–675 (1999).
[3] C.R. Jung, A. Kunddu, B. Ku, J.H. Gil, H.R. Lee and J.H. Jang, J. Power Sources, 175, 490–494 (2008).
[4] L. Soler, J. Macanas, M. Munoz and J. Casado, J. Power Sources, 169, 144–149 (2007).
[5] L. Soler, A.M. Candela, J. Macanas, M. Munoz and J. Casado, J. Power Sources, 192, 21–26 (2009).
[6] R. Orland, F.J. Torres, F. Pascale, P. Ugliengo, C. Zicovich-Wilson and R. Dovesi, J. Phys. Chem. B, 110, 692–701 (2006).
[7] M. Schoenitz and A. Navrotsky, Am. Miner., 84, 389–391 (1999).
[8] J. Duan and J. Gregory, Adv. Colloid Interface Sci., 100–102, 475–502 (2003).
[9] B.C. Bunker, G.C. Nelson, K.R. Zavadil, J.C. Barbour, F.D. Wall, J.P. Sullivan, C.F. Windisch Jr., M.H. Engelhardt and D.R. Baer, J. Phys. Chem. B, 106, 4705–4713 (2002).
[10] R.S. Alwitt, in Oxides and Oxide Films, Ed. by J.W. Diggle and A.K. Vijh, Marcel Dekker, New York (1976), Chapter 3.